Ferroelectric precursor behavior in $PbSc_{0.5}Ta_{0.5}O_3$ detected by field induced Resonant Piezoelectric Spectroscopy

Oktay Aktas,[1] Ekhard K. H. Salje,[1] Sam Crossley,[2] Giulio I. Lampronti,[1]
Roger W. Whatmore,[3] Neil D. Mathur,[2] and Michael A. Carpenter[1]

[1]*Department of Earth Sciences, University of Cambridge,*
Downing Street, Cambridge CB2 3EQ, UK

[2]*Department of Materials Science, University of Cambridge,*
Pembroke Street, Cambridge CB2 3QZ, UK.

[3]*Department of Materials, Royal School of Mines,*
South Kensington Campus, Imperial College London, London SW7 2AZ, UK

(Dated: November 5, 2013)

Abstract

A novel experimental technique, resonant piezoelectric spectroscopy, RPS, has been applied to investigate polar precursor effects in highly (65%) B-site ordered $PbSc_{0.5}Ta_{0.5}O_3$ (PST), which undergoes a ferroelectric phase transition near 300 K. The cubic- rhombohedral transition is weakly first order, with a coexistence interval of ∼4 K, and is accompanied by a significant elastic anomaly over a wide temperature interval. Precursor polarity in the cubic phase was detected as elastic vibrations generated by local piezoelectric excitations in the frequency range 250 kHz-710 kHz. The RPS resonance frequencies follow exactly the frequencies of elastic resonances generated by conventional resonant ultrasound spectroscopy, RUS, but RPS signals disappear on heating beyond an onset temperature, $T_{\rm onset}$, of 425 K. Differences between the RPS and RUS responses can be understood if the PST structure in the precursor regime between $T_{\rm onset}$ and the transition point, $T_{\rm trans}$ = 300 K, has locally polar symmetry even while it remains macroscopically cubic. It is proposed that this precursor behaviour could involve the development of a tweed microstructure arising by coupling between strain and multiple order parameters, which can be understood from the perspective of Landau theory. As a function of temperature the transition is driven by the polar displacement, P, and the order parameter for cation ordering on the crystallographic B-site, $Q_{\rm od}$. Results in the literature show that, as a function of pressure, there is a separate instability driven by octahedral tilting for which the assigned order parameter is Q. The two mainly displacive order parameters, P and Q, are unfavorably coupled via a biquadratic term, Q^2P^2, and complex tweed-like fluctuations in the precursor regime would be expected to combine aspects of all the order parameters. This would be different from the development of polar nano regions which are more usually evoked to explain relaxor ferroelectric behavior, such as occurs in PST with a lower degree of B-site order.

I. INTRODUCTION

Lead-based relaxor ferroelectrics with the perovskite structure are expected to play a major role as device materials, taking advantage of their outstanding dielectric, electro-optic, pyroelectric[1] and piezoelectric properties.[2] They are described as relaxors because their dielectric anomaly in the transition region is frequency dependent.[3,4] The physical reasons for such dispersion effects are usually described[5] as being due to polar nano regions (PNR's), which exhibit life times on the microsecond scale at temperatures near the dielectric permittivity maximum $T_{\rm m}$. Two additional important temperatures characterize the temperature evolution of PNR's, namely $T_{\rm d}$ and T^*. $T_{\rm d}$ is the Burns temperature where dynamic PNR's first appear,[6] while T^* is the temperature below which they start to correlate and become quasistatic.[7–9] In this approach, the PNR's are the defining structural elements of a traditional relaxor ferroelectric.[10] One may ask, however, whether PNR's are really needed or whether softer structural distortions may suffice to produce similar properties.[11] The question also arises as to what happens to PNR's when chemical disorder is too small to generate relaxor behavior. We will argue in this paper that local tweed structure might replace PNR's when the degree of B-site order is large. A typical example is the paraelectric phase of $BaTiO_3$ where local symmetry breaking is traditionally associated with PNR's while tweed-like structures have recently been evoked.[12] The conceptual difference between PNR's and tweed is illustrated in Fig. 1 where PNR's[13] are patchy while tweed[14] consists of interwoven incommensurate structures that contain locally polar regions as part of a complex wave pattern.

In order to investigate tweed and PNR's, we focus on the elastic properties of ferroelectric $PbSc_{0.5}Ta_{0.5}O_3$ (PST) with a relatively high degree of B-site order ($Q_{\rm od} = 0.65$). This material was chosen because its dielectric anomaly shows relaxor behavior[15–22] when the degree of B-site order is low but becomes a classic ferroelectric when the degree of structural order is high.[16–18,23] Our sample shows the classic ferroelectric transition but maintains sufficient Sc/Ta disorder to allow the formation of tweed structures (for review of the tweed mechanisms and the role of structural disorder see Refs. 24–26).

The ferroelectric phase transition near 300 K in highly ordered PST was first reported by Stenger et al.[16–18] and Setter and Cross.[19] It leads to a change in crystal structure from a paraelectric cubic phase with space group $Fm\bar{3}m$ to a ferroelectric rhombohedral

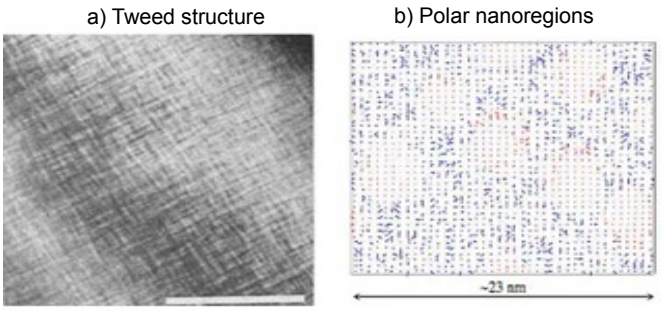

FIG. 1. Comparison of tweed structures and polar nanoregions (PNRs). **a)** An electron micrograph of tweed structures observed in $YBa_2(Cu_{1-x}Co_x)_3O_{7-\delta}$. Scale bar corresponds to 0.1 μm (reprinted by permission of the publisher (Taylor & Francis Ltd, http://www.tandf.co.uk/journals) from Ref. 14, Schmahl et al., Philos. Mag. Lett. **60**, 241 (1989).) **b)** A simulation of PNR's. The horizontal dimension of the image corresponds to 23 nm (Reprinted with permission from Ref. 13, B. P. Burton, E. Cockayne, and U. V. Waghmare, Phys. Rev. B **72**, 064113 (2005). Copyright (2013) by the American Physical Society).

phase with reported space group $R3$.[19,20,23,27–31] The transition is close to tricritical but slightly first order in character,[16–19,27,29,32] such that the transition temperature, $T_{\rm trans}$, is only slightly different from the critical temperature, $T_{\rm c}$, and there is a small coexistence interval. $T_{\rm trans}$ shifts to lower temperatures with increasing B-site disorder,[15–18,20,27] and, for example, is near 260 K in PST with 8% order ($Q_{\rm od} = 0.08$).[21] Even very low B-site order is not enough to prevent the macroscopic electric polarization from becoming established at low temperatures.[16,18,27,33] The maximum of the dielectric constant also shifts to lower temperatures, but there is a crossover between ordered samples which display only the ferroelectric transition, with $T_{\rm m} \sim T_{\rm trans}$, and disordered samples which also show the frequency dependent dielectric maximum characteristic of relaxor behavior, with $T_{\rm m} > T_{\rm trans}$.[16–18,23,27,33] An incommensurate antiferroelectric (IAFE) structure has also been reported to coexist with the paraelectric and ferroelectric states in single crystals of PST in the temperature range 223 K-323 K. This structure is a major component only when the degree of order is greater than 90% but was not found in ceramic samples.[23] Reported values for the characteristic temperatures T^* and $T_{\rm d}$ in PST with low $Q_{\rm od}$ are 450 K-500 K and ∼700 K, respectively.[9,15,20,22,34]

We describe for the first time an experimental technique, resonant piezoelectric spec-

troscopy, RPS, which allows us to detect polar short range order over a large temperature interval in highly B-site ordered PST. RPS measurements were complemented by x-ray diffraction, dielectric constant, ferroelectric hysteresis, and resonant ultrasound spectroscopy (RUS) measurements. Our data for a sample with $Q_{\mathrm{od}} = 0.65$ show that a distinct regime extends between 300 K and 425 K, in which precursor effects are related to the fluctuations of state parameters as formulated by the fluctuation-dissipation theorem.[35] The origin of these fluctuations can be conveniently described using Landau theory. Therefore, we developed a phenomenological Landau model with ferroelastic and ferroelectric order parameters, B-site ordering, heterogeneities inherent to the sample, and coupling between these order parameters allowed according to group theory (but possible incommensurate or antiferroelectric order parameters are not considered). It leads, in particular, to a model in which the polar precursor effects observed in highly ordered PST can be characterized by both octahedral distortions and cation off-centering. In addition, all the experimental observations of this precursor ordering are compatible with polar tweed patterns when the B-site ordering is high, in contrast with the dominance of classic PNR's when the B-site order is low.[9,16–18] We determine an onset temperature, T_{onset}, for these precursor effects as 425 K, which is the temperature at which the RPS signal (or local polar ordering in the possible tweed patterns) disappears on heating.

II. RESONANT PIEZOELECTRIC SPECTROSCOPY, RPS

The characteristic feature of RPS is that standing elastic waves are excited by a weak electric field applied to the sample (see Fig. 2). The field leads to local lattice deformation through a local piezoelectric effect. The deformations then form elastic waves which, when they become resonant standing waves, penetrate the entire sample. The resonant vibrations are detected by piezoelectric receivers (acoustic detectors) which are mounted at the far end of a ceramic rod that touches the sample and transmits any elastic signal emitted from the sample to the receiver. This 'listening rod' acts as the detector of any electrically excited waves in the sample. Only piezoelectric materials can emit such waves, but the piezoelectric effect need not be macroscopic and can relate to small local regions that deform elastically under an external electric field. It is only required that a finite piezoelectric component exists after averaging over the wavelength of the standing wave. One advantage of this technique

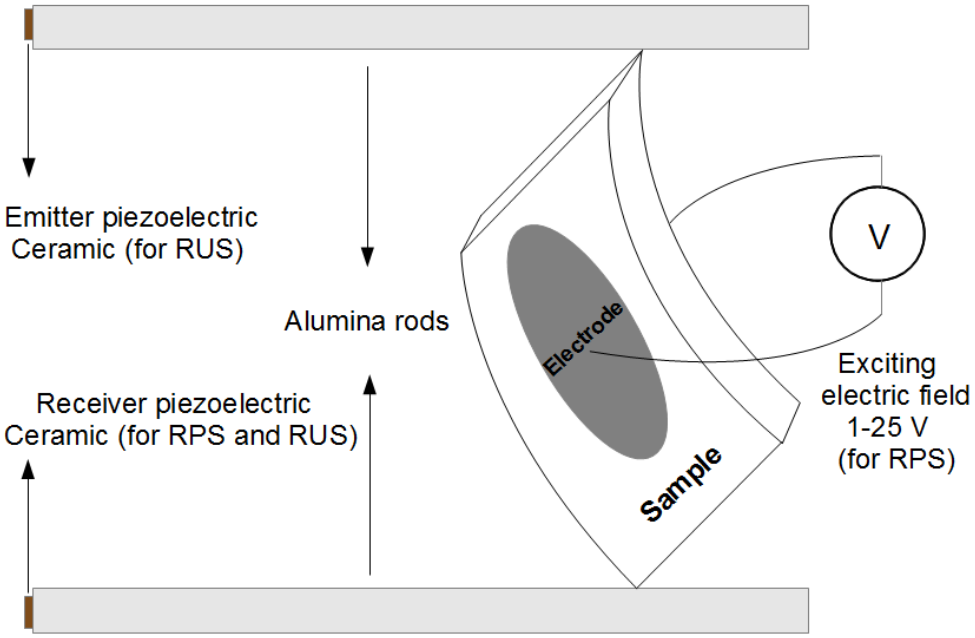

FIG. 2. Schematic view of the experimental configuration used for resonant piezoelectric spectroscopy (RPS).

is its enormous sensitivity: as long as a standing wave can be excited, its frequency can be measured rather easily. Elastic resonances of samples with elastic constants typical of oxides and with dimensions of a few mm occur between 100 kHz and 10 MHz and can be measured with a resolution in frequency of $\sim$1 Hz.

The sample can be of arbitrary shape and for high temperature and low temperature measurements can be easily located inside a furnace or a cryostat. The exciting electric field is typically 1-25 V and the receiver signal is split into the amplitude and phase of the standing wave (or the in-phase and out-of-phase signal of the receiver). Additional resonance peaks, referred to as rod peaks, in RPS spectra from the experimental set up shown in Fig. 2 for measurements at high temperatures are due to standing waves in the alumina receiver rod, but as this rod is partially inside and partially outside the furnace the frequencies do not change significantly with temperature. Their amplitude, on the other hand, originates from the piezoelectric effect of the sample so that the amplitude of a rod peak is a good measure for the piezo-coefficient of the sample. In general, the piezoelectric effect of the sample can be separated very clearly from mechanical or electric background excitations and can serve as a very sensitive detector for piezoelectricity in samples with a variety of

sizes and shapes.

RPS is an experimental technique very closely related to Resonant Ultrasound Spectroscopy, RUS, in which standing waves are excited externally by a piezoelectric emitter, usually a poled PZT ceramic.[36] In the experimental arrangement shown in Figure 2 this emitter transducer is attached to the end of the second alumina rod. Both transducers sit outside the furnace used for heating experiments.[37] Switching from RPS to RUS is achieved simply by applying the AC voltage across the emitter transducer rather than across the sample. It is worth noting that both RUS and RPS probe essentially the same mechanical resonances, and reveal the elastic properties of the sample.[12,38–41] However, RPS is a result of polar properties of the sample at a macroscopic and/or microscopic scale (i.e. polar nanostructures).

III. SAMPLE CHARACTERIZATION AND EXPERIMENTAL METHODS

PST ceramic samples were fabricated using the mixed-oxide method described by Osbond and Whatmore.[42] Sc_2O_3 and Ta_2O_5 powders were milled together and then pre-reacted at 900°C to form the wolframite phase $ScTaO_4$. This was then reacted with PbO at 900°C to form a single-phase perovskite powder, which was subsequently hot-pressed in Si_3N_4 tooling and an alumina grit packing medium at 40 MPa and 1200°C for 6 hours. All the samples used in our experiments were cut from a larger cylindrical piece with a thickness of ∼1 mm. Samples from the same batch were previously used to describe the field and temperature dependence of the dielectric properties of this material.[43,44] The chemical composition was checked by microprobe analysis which indicated good uniformity of the Sc and Ta concentration and small (2%) variations for Pb.

X-ray diffractograms in the 2θ range 10°-120° were collected in air in Bragg-Brentano geometry on a D8-ADVANCE diffractometer equipped with an MRI high-temperature chamber using Cu Kα radiation, a Göbel mirror for the parallel primary beam, and a Vantec linear position sensitive detector. A sample with an area of $\sim 1\times \sim 1$ cm^2 was put in the high temperature chamber to obtain the x-ray diffractograms between 300 K and 840 K. Rietveld refinements were performed with the software Topas V4.1.[45] The value of the long range chemical order parameter $Q_{\rm od}$ was calculated as 0.65 using the equation $Q^2_{\rm od} = (I_{111}/I_{200})/(I_{111}/I_{200})_{(Q_{\rm od}=1)}$, where I_{111} and I_{200} correspond to powder x-ray

diffraction intensities for the cubic (111) and (200) Brag peaks; $(I_{111}/I_{200})_{(Q_{od}=1)} = 1.33$ for complete order.[17,31]

RUS measurements above room temperature were performed using a Netzsch 1600°C furnace, as described by McKnight et al..[37] The same furnace was also used for RPS measurements. Exciting AC voltages of ∼20 V and 10 V were applied across the sample and the emitter transducer for the RPS and RUS measurements, respectively. An Orange 50 mm helium flow cryostat was used for low temperature RUS measurements, as also described in detail elsewhere.[46] The exciting AC voltage applied across the emitter transducer was 25 V. The sample used in RUS and RPS experiments had dimensions of $\sim 7\times \sim 7\times \sim 0.5$ mm^3.

In the high temperature experiments all RPS and RUS spectra were collected during heating sequences from 300 K. In the low temperature experiments RUS spectra were collected between 200 K and 310 K during both heating and cooling. A DC voltage of 600 V was applied across the sample electrodes prior to RPS measurements. RUS measurements were performed both before and after applying the same voltage to the sample. A settle time for thermal equilibration was allowed before data collection at each temperature, depending on the temperature steps. For measurements performed every 0.2-0.4 K around the transition temperature, this settle time was 90 seconds while, for measurements performed every 5 K, it was 20 minutes. RUS and RPS spectra were collected in the frequency range from 250 kHz to 710 kHz and then analyzed using the software package IGOR PRO (WaveMetrics). Peak frequencies and full widths at half maxima (FWHM) of selected resonance peaks were determined by fitting with an asymmetric Lorentzian profile. The square of a resonant frequency scales with the effective elastic modulus associated with that mode. For a polycrystalline sample, as used in the present study, the effective elastic modulus would be a combination of the bulk modulus and shear modulus. Most low frequency modes measured are dominated by shearing, but a few have non-volume preserving components. Damping is expressed in the form of the inverse mechanical quality factor, Q^{-1}, which is taken to be $\Delta f/f$, where f is the peak frequency and Δf the full width at half maximum height of the resonance peak. In what follows Q^{-1}, the inverse mechanical quality factor, is easily distinguished from Q, the order parameter for octahedral tilting, by the context.

For dielectric measurements, the sample, which was also used for the RUS and RPS measurements, was mechanically polished to a thickness of ∼450 μm. Its largest surfaces were electroded with Au/Cr and silver paste was applied to the electrodes. Then, it was

mounted in vacuum on a copper heat reservoir in a probe that was inserted into liquid nitrogen. Impedance spectra were collected using an Agilent 4294A analyzer between 40 Hz and 100 kHz. The capacitance of the sample was estimated using a parallel equivalent circuit model. Hysteresis loops of polarization versus electric field ($P(E)$) were measured at various temperatures near the ferroelectric transition temperature at 1 Hz with driving voltages of ∼1000 V using a Radiant Precision Premier II tester and external amplifier (Trek 609E-6). The sample used to measure the $P(E)$ curves had a thickness of 420 μm and a Pt electrode area of 0.29 cm^2.

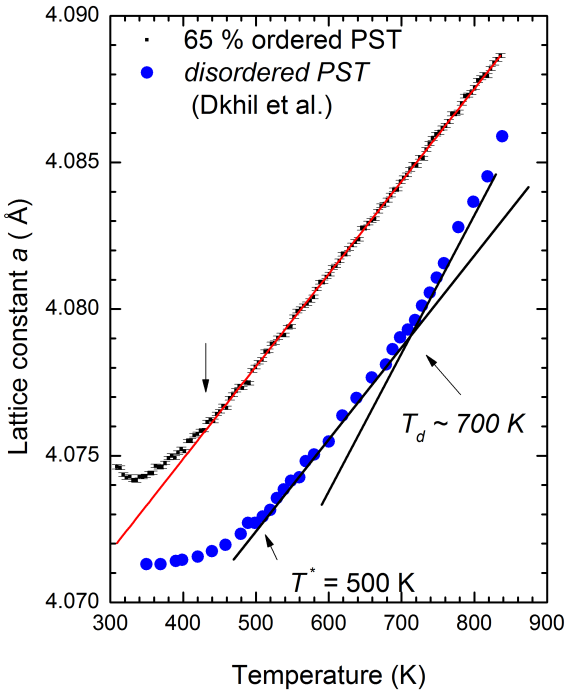

FIG. 3. Temperature evolution of the pseudocubic lattice parameter of the reduced unit cell in the $Fm\bar{3}m$ phase of $PbSc_{0.5}Ta_{0.5}O_3$ with $Q_{od} = 0.65$. The red line is a linear fit to the data. The black arrow is placed at 425 K to indicate where the break from a linear trend occurs. Lattice parameter data for $PbSc_{0.5}Ta_{0.5}O_3$ with an unspecified degree of order from Dkhil et al.,[9] are included for comparison (filled blue circles).

IV. RESULTS

The cubic lattice parameter for the primitive unit cell of the sample used in this study was found to be 0.407462 ± 0.000008 nm at 300 K, which is similar to previously reported values (0.40837 nm,[30] and 0.40766 nm[29]). The temperature-dependence of the reduced unit cell parameter is shown in Fig. 3, showing linear thermal expansion (continuous line) from 840 K down to 425 K. Between 425 K and 300 K, the variation is non-linear and there is a minimum at 330 K. This temperature dependence is different from that obtained for a PST sample with an unspecified degree of order by Dkhil et al..[9] As shown in Fig. 3, the data reproduced from Dkhil et al. show two breaks in slope. The first is located near 700 K and is associated with Burns temperature, $T_{\rm d}$, and the second is at $T^* = 500$ K. Dkhil et al.[9] claimed that T^* is invariant for most Pb-based perovskites and independent of the degree of B-site ordering, but there is no evidence for an anomaly at either ∼500 K or ∼700 K in the temperature evolution of the lattice constant in our ordered sample. Rather, the precursor change in thermal expansion has an onset at ∼425 K for our sample, which is well below all anomalies reported by Dkhil et al..[9] Similar data reported by Mihailova et al.[34] has the onset of non-linear expansion at ∼450 K. If this is the same sample as described by Dul'kin et al.,[21] Maier et al.,[47], and Mihailova et al.[48] as appears to be the case, it has $Q_{\rm od} =$ 0.08 based on refinements of site occupancies or 0.13 based on the intensity ratios of Bragg reflections and a ferroelectric transition at 261 K.[21]

Segments of the primary RUS and RPS spectra are shown in Figs. 4a and b, respectively. The y-axis should be amplitude, in volts, from the amplifier but the spectra have been translated vertically in proportion to the temperature at which they are collected and the y-axis relabeled as temperature. RUS spectra collected between 200 K and 785 K show a characteristic dip in resonance frequencies near the ferroelectric transition (300 K). RPS spectra measured in the stability field of the macroscopically cubic phase show exactly the same trend of stiffening with increasing temperature as the RUS spectra. The electrically induced resonance frequencies obtained by RPS in fact coincide with RUS frequencies, showing that RPS generates the same mechanical resonances as obtained when the driving mechanism is the emitter transducer in RUS. This is clearly seen for the peak located at about 452 kHz in both the RUS and RPS spectra, indicated by blue arrows between 370 K and 425 K in Figs. 4c and d. Note that peaks located below 420 kHz, with the exception of the peak lo-

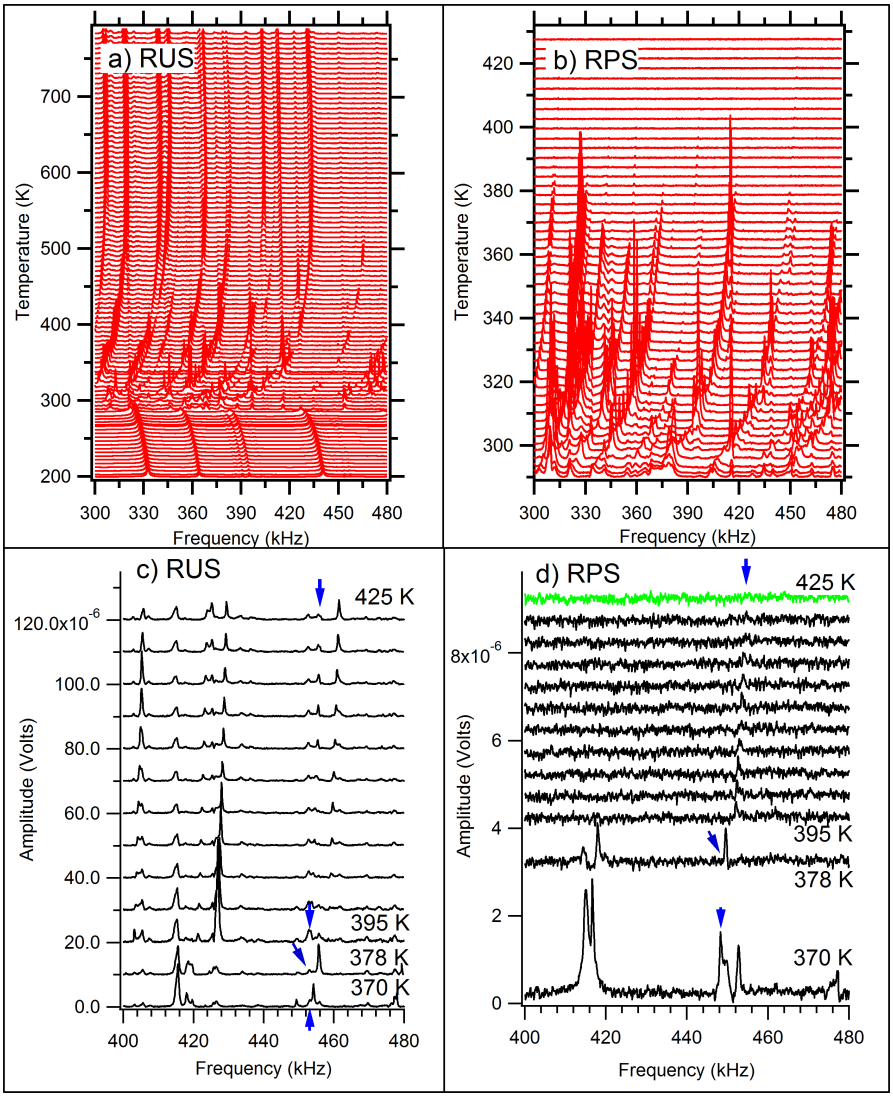

FIG. 4. **a)** RUS Right: **b)** RPS spectra of $PbSc_{0.5}Ta_{0.5}O_3$ at high temperature. The left axis is the amplitude (in Volts) but the spectra have been offset in proportion to the temperature at which they were collected. The axis is labeled accordingly. **c)** Some RUS spectra collected between 370 K and 425 K. **d)** Some RPS spectra collected between 370 K and 425 K. The blue arrows in parts **c)** and **d)** indicate the temperature evolution of the same sample resonance peak.

cated at 418 kHz at 470 K, with frequencies which have almost no temperature-dependence are resonance modes of the alumina rods. All peaks above 420 kHz in Figs. 4c and d are from resonances of the PST sample and their frequencies increase with increasing temperature. One notable difference between RUS and RPS spectra is that the amplitudes of peaks collected by RUS have larger amplitudes than those collected by RPS. In addition, while peaks

in RUS spectra exist in all spectra, peaks in RPS spectra reduce in amplitude and eventually fade into the background on heating. For example, the RPS spectrum at 395 K has only one peak (f∼452 kHz, indicated by an arrow in Fig. 4d) that can be distinguished from the background. At 425 K, this peak is no longer discernible and we argue that $T_{\rm onset}$ = 425 K is the characteristic temperature where polarity starts on cooling. This is the same as the temperature at which the cubic lattice parameter shows the deviation from linear thermal expansion (Fig. 3).

Data for a single resonance peak in the RUS and RPS spectra are combined in Fig. 5. The blue open circles are frequencies from RUS measurements, plotted as f^2 which scales essentially with the shear modulus. They show a dip at the transition point, as shown in the inset of Fig. 5. The red full circles are frequencies from the same peak in the RPS spectra, which disappears above 425 K. Damping, represented by variations of the inverse mechanical quality factor, Q^{-1}, is shown as stars (RUS) and number symbols (RPS). Damping is low in the cubic phase and only slightly higher in the rhombohedral phase. The evolution of Q^{-1} around the transition temperature is also shown in the inset of Fig. 5. The damping mechanism has been simulated by Ding et al.[49] and relating their results to the observations

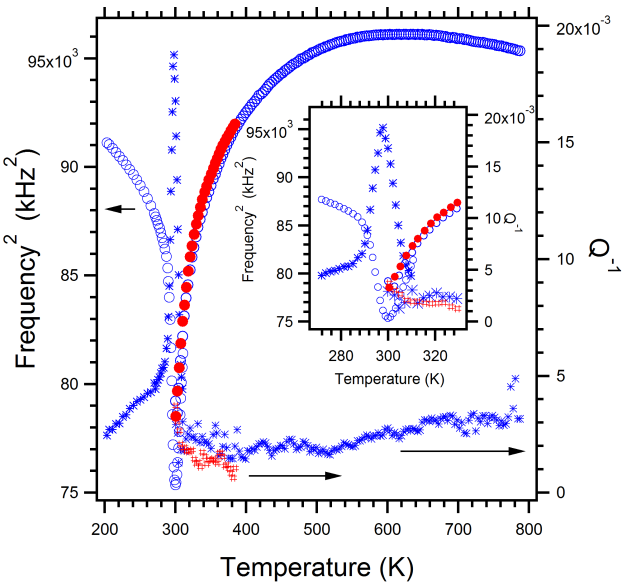

FIG. 5. Temperature-dependence of the square of mechanical resonance frequencies and the inverse quality factor obtained for a single resonance peak from RUS and RPS spectra of $PbSc_{0.5}Ta_{0.5}O_3$. RUS data for f^2 and Q^{-1} are shown with blue open circles and stars, respectively; RPS data are represented by red filled circles and number symbols.

indicates that no macroscopic microstructures (such as extended twin structures) exist in the cubic phase. Local symmetry-breaking, either as frozen defects or as long-wavelength deformations, must exist, however, as testified by the RPS signal. Chemical heterogeneities on a 100 nm scale do not seem to restrain the movement of polar displacements on a much smaller 10 nm scale.[29] Near the transition point we do find a strong increase of the damping, which is typical for the movement of phase boundaries which contain strong friction at grain boundaries or with other microstructures.[50] The dip in f^2 is much smaller than the equivalent anomalies associated with transitions in other perovskite structures such as $SrTiO_3$,[51] $BaTiO_3$,[12]or $KMnF_3$.[52]

Fig. 6 shows the dielectric anomaly measured at three different frequencies, 100 Hz (red line), 1 kHz (blue line), and 100 kHz (green line). The dielectric constant shows a maximum at 300 K for all frequencies, although its amplitude depends on the frequency of the applied field. Fig 6 also displays the collapse of the average of the piezoelectric coupling coefficient,

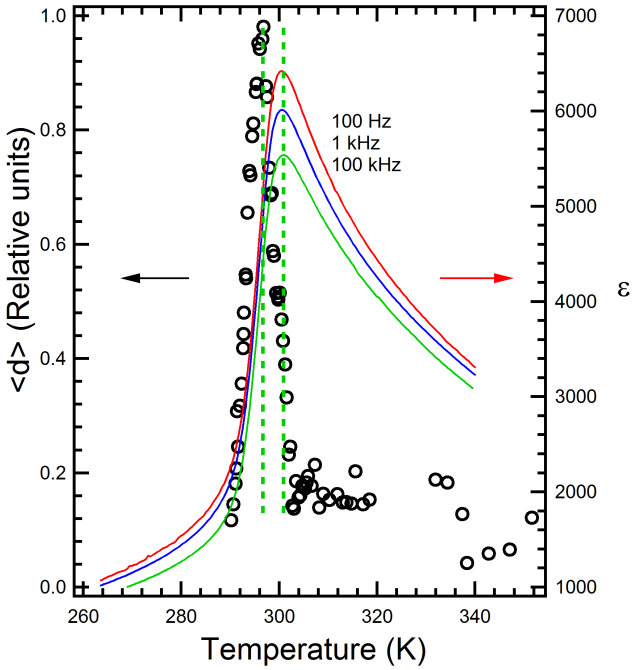

FIG. 6. Variation of the space averaged piezoelectric coefficient $< d >$ (open circles) and dielectric constant, ϵ, measured at 100 Hz, 1 kHz, and 100 kHz (red, blue, and green curves, respectively,) with temperature across the cubic-rhombohedral phase transition. Maxima in $< d >$ and ϵ occur at 296 K and 300 K, respectively.

$< d >$ at the transition point. Here, $< d >$ is the amplitude of a rod peak calculated using a fit to the data with an asymmetric Lorentzian function. Since the rod peaks are excited through piezoelectric coupling in the sample, values of $< d >$ are proportional to the piezoelectric coefficient. It is also worth noting that the voltage across the sample electrodes around the dielectric peak point changed by almost 25% due to changes in the dielectric constant of the sample. As a result, $< d >$ actually exhibits a sharper peak profile than that shown in Fig. 6. The peak in ϵ is at 300 K while $< d >$ has its maximum at 296 K. The collapse of $< d >$ then extends over the coexistence interval between 296 K and 300 K. The reduction in $< d >$ and details in the temperature-dependence of ϵ are consequences of the averaging procedures in the phase mixing interval which are different for the two quantities.[3] RUS and dielectric measurements show a thermal hysteresis, indicating a first order transition, in agreement with earlier studies,[16–18,29,32] though only data collected during heating are shown in Figs. 5 and 6.

Fig. 7 shows $P(E)$ loops obtained at 1 Hz with driving voltages near 1000 V. A typical ferroelectric hysteresis is seen at 290 K. Increasing temperature leads to an apparent double hysteresis loop at $T >$300 K. The loops move out from the origin as the transition becomes harder to drive, clearly indicating that the double-hystereses loops represent a field-induced phase transition to the ferroelectric phase. Field-induced double hysteresis loops have also previously been measured in highly disordered PST.[27] Double hysteresis loops have been observed in other ferroelectric compounds including $BaTiO_3$[53] and 8.2/70/30 (La/Zr/Ti atomic %) PLZT (lanthanum modified lead zirconate/lead titanate).[54]

We can now estimate the characteristic temperatures of the phase transition and compare them with other values reported for PST. During heating, the onset of the interval where the rhombohedral and cubic phases coexist is 296 K. With increasing temperature, the fraction of the paraelectric cubic phase increases, while that of the ferroelectric rhombohedral phase diminishes, which leads to the collapse of space averaged piezoelectric coefficient $< d >$. (Fig. 6). At $T >$ 300 K the rhombohedral phase is not visible by x-ray diffraction, so that this temperature has been taken as the upper stability point of the ferroelectric phase. For clarity, dashed green lines are shown in Fig. 6 to indicate this coexistence interval. The actual transition temperature $T_{\rm trans} = 300$ K is estimated from the maximum of the dielectric response, and this coincides with the temperature at which the mechanical resonance frequency is at a minimum. From the RPS measurements, the onset temperature

for polar regions is at a much higher temperature, 425 K, which is consistent with the change from linear to non-linear thermal expansion (Fig. 3).

While our data do not correlate with the determination of $T^* = 500$ K by Dkhil et al.,[9] we find that the onset temperature for polar precursors is closer to $T^* = 450$ K specified by Sivasubramanian and Kojima[20] as being the temperature below which a central peak appeared and line broadening of the peak from a longitudinal phonon mode started in Brillouin spectra from a sample with $Q_{\rm od} = 0.55$, 450-460 K given by Maier et al.[15] from a break in slope of frequency and linewidth of a Raman peak, and 450 K from acoustic emission experiments on a single crystal with $Q_{\rm od} = 0.08$.[22] This is indistinguishable from the temperature at which Mihailova et al.[34] reported a break in slope of the cubic lattice parameter with temperature, from a sample which is assumed to have been the same as used by Dul'kin et al. ($Q_{\rm od} = 0.08$).[21]

The crossover from relaxor behavior to more classical ferroelectric behavior is most easily defined as the degree of order where $T_{\rm m}$ and $T_{\rm trans}$ coincide. From the earliest measurements of Stenger et al.[16] this occurs between $Q_{\rm od} = 0.74$ and 0.82. However, although Sivasubramanian and Kojima[20] reported a weak dispersion in their low frequency dielectric data and, hence, "a weak relaxor-like behavior" for their sample with $Q_{\rm od} = 0.55$, the maximum in the real part of the dielectric constant at 297 K is independent of frequency in their Fig. 2 (as in Fig. 6) and is also close to the value of $T_{\rm trans} = 295$ K specified on the basis that this is

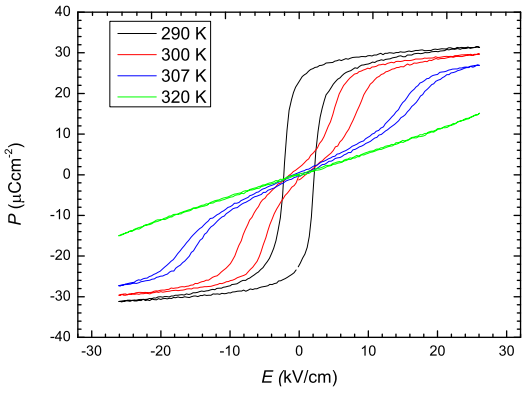

FIG. 7. $P(E)$ loops at 1 Hz obtained using a 420 μm thick $PbSc_{0.5}Ta_{0.5}O_3$ sample at 290 K (black line), 300 K (red line), 307 K (blue line), and 320 K (green line).

the temperature at which there is a sharp minimum in the frequency and a sharp maximum in the width of a longitudinal acoustic phonon peak. This would put the crossover between samples with relaxor ferroelectric character ($T_{\rm trans} < T_{\rm m}$) and samples which display only a ferroelectric transition ($T_{\rm trans} \sim T_{\rm m}$) on the disordered side of $Q_{\rm od} = 0.55$, consistent also with a high transition temperature, $T_{\rm trans} = 295$ K, for the sample of Woodward and Baba-Kishi[29] which had $Q_{\rm od} = 0.52$. The sample investigated in the present study has $T_{\rm trans} \sim T_{\rm m}$ and is on the ordered, ferroelectric side of the crossover.

The other phase transition which can occur in PST is from the paraelectric state to an incommensurate antiferroelectric structure IAFE.[23,55] Although Baba-Kishi and Pasciak[23] found the stability limits for this structure to be ∼223-323 K and only in single crystals with $Q_{\rm od} > 0.85$, Dul'kin et al.[21] observed an acoustic emission peak at 293 K from a sample with $Q_{\rm od} = 0.08$ which they attributed also to the appearance of the IAFE structure. Neither in the present study ($Q_{\rm od} = 0.65$), nor in that of Sivasubramanian and Kojima[20] ($Q_{\rm od} = 0.55$) has any evidence for changes in elastic or anelastic properties been found in these temperature ranges other than the anomalies ascribed to the $Fm\overline{3}m - R3$ transition, however. In addition, the shape and the temperature evolution of $P(E)$ loops shown in Fig. 7 indicate that the double hysteresis loops are due to a field-induced ferroelectric state and do not support the appearance of an antiferroelectric phase. The only possible correlation with the present data might be that the minimum in the cubic lattice parameter at ∼330 K in Figure 3 is related to the appearance of some kind of incommensurate and/or antiferroelectric ordering. On the other hand, Brillouin data from a crystal with $Q_{\rm od} = 0.29$ show two features, a broad minimum of the elastic constants C_{11} and C_{12} in the vicinity of $T_{\rm m} \sim 280$ K, and a sharp anomaly at ∼297 K in the width and integrated intensity of the Brillouin peak from a longitudinal acoustic mode.[56] There is certainly some structural change occurring near 295 K in relatively disordered samples, but it does not obviously relate to the onset of local polarity in relatively ordered samples observed by RPS in this study.

V. ORDER PARAMETER COUPLING AND MICROSTRUCTURE

We use Landau theory to disentangle the various contributions to structural phase transitions and the precursor order. The motivation for this is to consider the implications of multiple instabilities in PST for the stability and properties of possible microstructures, in

particular the formation of a tweed microstructure. A first attempt to analyse the combined order parameters was undertaken by Salje and Bismayer,[57] who dissected the transition into its ferroelastic, ferroelectric, and B-site ordering components. Sivasubramanian and Kojima[20] analyzed the results of Brillouin scattering experiments and the observation of a central peak in terms of a simplified Landau potential where the transition was represented as a single event without further considerations of the symmetry constraints. Their order parameter was the spontaneous polarization, which couples with the lattice strain in a quadratic-linear fashion. They included a bilinear coupling between the order parameter and strain but this is disallowed by symmetry in the simplest case of improper ferroelectric behavior.

The temperature dependence of the symmetry-breaking rhombohedral strain follows the pattern typical of a phase transition which is close to tricritical in character, but is weakly first order, in a sample with $Q_{\rm od} = 0.52$[29] and in a sample which is presumed to have $Q_{\rm od} = 0.08$.[34] Both sets of data also show a quantum saturation[26] effect below $T_S \sim 80$K which would calibrate the quantum saturation temperature $\Theta_S = 2T_S$ to ∼160 K, as is rather typical for perovskite structures.[58,59] In addition to temperature-induced transitions there are transitions as a function of pressure.[30,47,60–62] With increasing pressure at room temperature in a crystal with $Q_{\rm od} = 0.08$, the cubic structure becomes rhombohedral between 1 and 2 GPa, predominantly by the appearance of octahedral tilting, and apparently without ferroelectric ordering.[30] The change in space group for this paraelectric/paraelastic→paraelectric/improper ferroelastic transition was reported to be $Fm\overline{3}m \rightarrow R\overline{3}$, and the square of the refined tilt angle was found to be a linear function of pressure, consistent with second order character.

We represent tilts by the displacive order parameter Q, B-site order by $Q_{\rm od}$, and ferroelectric order by P, which belong to irreducible representations R_4^+, R_1^+, and Γ_4^-, respectively, of the parent space group, $Pm\overline{3}m$. All other possible structural instabilities (such as the claimed antiferroelectric and/or incommensurate transitions) are ignored because they do not relate to the observed piezoelectric effect. Furthermore, the proposed tweed structures do not require any instability outside the Γ-point. In principle, symmetry breaking can be described as a cumulative process with the potential structural forms $Pm\overline{3}m$ ($Q_{\rm od} = 0$, $Q = 0$, $P = 0$), $Fm\overline{3}m$ ($Q_{\rm od} \neq 0$, $Q = 0$, $P = 0$), $R\overline{3}$ ($Q_{\rm od} \neq 0$, $Q \neq 0$, $P = 0$), $R3m$ ($Q_{\rm od} \neq 0$, $Q = 0$, $P \neq 0$), $R3$ ($Q_{\rm od} \neq 0$, $Q \neq 0$, $P \neq 0$).[29] For the construction of the Landau

potential the enlarged intermediate cell of $Fm\bar{3}m$ is important because the critical point can be $\Gamma(k = 0)$ for the uniform (non-relaxor) state. The ferroelectric transition is improper because the active irreducible representation of the octahedral tilts does not contain a representation of the symmetry breaking spontaneous strain.[63] In reality, the structure of the low temperature ferroelectric phase may be more complicated than this simple analysis would imply since Woodward and Baba-Kishi[29] required an enlarged unit cell to account for all the weak reflections that appeared in their diffraction patterns. Octahedral tilting is allowed under $R3$ symmetry in their structure, but is not observed. There nevertheless appear to be R_4^+ contributions in the form of distortions of the octahedra. For present purposes it is sufficient to consider the three order parameters of the ideal case.

We assume that all order parameters are strongly coupled. The elastic anomaly stems from the additional coupling between the order parameters and the elastic strain e, which, in turn, determines the elastic moduli.[52] The elastic part of the Gibbs energy is then $L(Q) + G(e) + G(Q, e)$. We write the ferroelectric component as $L(P) - PE$ where the ferroelectric order parameter is P (the spontaneous polarization) and E is the applied electric field. In this approach, P includes the simple ferroelectric displacement. The reported additional symmetry breaking from $R3m$ to $R3$, due to the R_4^+ order parameter without a contribution from tilting, is not considered in this scheme and may be due to another order parameter e_{flip}, possibly related to electronic effects of the off-centering of Pb. Such local distortions of Pb inside high symmetry cages were observed previously in $Pb_3(PO_4)_2$,[64,65] where they give rise to specific flip-mode excitations. Coupling between the ferroelectric order parameter P and the strains e_P and e_{flip} includes linear-quadratic terms which can greatly influence the stability of the individual phases.[66] If there was any possibility of bilinear coupling between a symmetry-breaking shear strain and P, precursor elastic softening which we observe experimentally would reflect a pseudo-proper transition mechanism[52] in addition to other softening mechanisms. However, as discussed below, this does not appear to be the case.

The Gibbs free energy is the superposition of all energies and the coupling between Q_{od}, Q and P, as set out in Eq. A1 of the appendix. This leads to the Landau potential in Eq. A14, which, with the gradient terms in Eqs. A2-A4 constitute the same coupled equations that were treated in Refs. 67 and 68 to show that twin boundaries in the tilt order parameter Q will always combine with breather solutions of the order parameter P. This means that

over a limited temperature and/or pressure interval close to the transition point of the high pressure phase transition to the ferroelastic tilt phase we expect polar states inside the twin boundaries (but not inside the bulk).[68] This implies that the domain walls have ferroic functionalities in the tilted phase and qualify as possible ferroelectric switching elements anchored inside the twin boundaries. The concept of such functional domain boundaries was discussed as 'domain boundary engineering' in Ref. 69. Examples for ferroic twin boundaries and the treatment by the Landau potential (Eq. A14) were discussed in Refs. 70–72. The first experimental observation was reported in the orthorhombic tilt phase of $CaTiO_3$.[73] The importance of PST is hence that it is potentially a functional material with localized polarity inside domain walls and could be used as a high density switching material if these domain walls could be addressed individually by electric fields.

In the Landau expansion developed in the appendix we allowed $Q_{\rm od}$ to be fixed, with Q and P relaxed accordingly and the coupled strain becoming $e_{\rm relax}$. If we assume that the most important coupling is between Q and P and is via $e_{\rm relax}$, the elastic constants will reflect an improper ferroelastic phase transition with biquadratic coupling, $\lambda P^2 Q^2$. Experimental data for lattice parameter variations show that this must be unfavourable, however. With falling temperature through the (tricritical/weakly first order) $Fm\overline{3}m \rightarrow R3$ transition the volume strain is positive (see Figure 5 of Ref. 29 and Figure 10 of Ref. 34, and the shear strain, $e_4 \approx \cos\alpha$, is positive (pseudocubic lattice angle $\alpha_R < 90°$). Increasing pressure stabilizes the paraelectric and octahedrally tilted structure and the (second order) transition $Fm\overline{3}m \rightarrow R\overline{3}$ is accompanied by a negative volume strain. The rhombohedral phase is reported to have $\alpha_R > 90°$ and, hence, e_4 is also negative (Table 2 of Ref. 30). Opposite signs for both of these symmetry-adapted strains must contribute to a tendency for increasing Q to cause suppression of P, and vice versa.

We now include heterogeneities in the Gibbs free energy with $g \neq 0$. A major deviation from the uniform state relates to the piezoelectric coefficients. Equation A13 defines the piezoelectric effect and relates the piezoelectric coefficient d to the order parameter P. This relationship holds in the uniform state only and fails when the sample become heterogeneous (such as in crystals with microstructures and particularly in the coexistence interval) where $< d >$ and $< e >$ have to be evaluated in effective medium theory.[74] Such heterogeneity clearly exists in the cubic phase of PST because the space averaged piezoelectric coefficient $< d >$ is nonzero over a large temperature interval above $T_{\rm trans}$ although in the cubic phase

d should be zero. A finite $< d >$ value in the cubic phase indicates the existence of a polar rhombohedral phase on a local scale, i.e. microstructures. The decay of $< d >$ hence shows that the proportion of rhombohedral regions in the cubic phase diminishes upon heating.

The introduction of the gradient energies in P, Q, and e lead inevitably to structural modulations. Each modulation alone would be symmetrical without coupling to the other order parameters. This means that $+\mathbf{P}$ and $-\mathbf{P}$ are equally likely in this scenario. However, coupling terms involving P^2, such as in Q^2P^2 and P^2e, are invariant relative to the sign of P and allow poling in weak fields by flipping P to the energetically favorable direction. This idea goes beyond the standard treatment of tweed structures[23–25,34,75,76] which is inspired by the fluctuation of atomic positions in a multi-valley energy landscape and the slaving of all other degrees of freedom, while here we find polarity as a coupling effect between P and other structural deformations. The results of previous tweed simulations remain unchanged by this addition, however.

The present Landau analysis could be extended to include an order parameter for antiferroelectric ordering but the essential points are, firstly, that the instabilities for tilting and ferroelectric ordering cannot be far different in energy and, secondly, that the two order parameters have particular characteristics which have implications for the properties and behavior of transformation-related microstructures. In particular, they have the potential to give rise to tweed in some pressure and temperature interval ahead of the symmetry-breaking critical points. The known occurrence of an incommensurate phase in samples with $Q_{\rm od} > 0.9$ is entirely consistent with the view that strain and order parameter gradients can stabilize modulated and tweed structures in PST.[24]

VI. PRECURSOR SOFTENING

A distinctive property of relaxor materials is softening of the elastic constants over a wide temperature interval below the Burns temperature. In the case of PMN, the Burns temperature is ∼630 K and the three symmetry adapted elastic constants, C_{11}, C_{12} and C_{44} all soften down to the freezing interval (e.g. see Fig. 9 of Ref. 41). This can be understood in the most general terms as being due to coupling of acoustic modes with relaxational modes of the dynamical PNR's which first appear at $T_{\rm d}$. The Burns temperature for PST has been given as ∼710 K on the basis of a change in thermal expansion,[9] ∼600 K on the basis of

an onset of elastic softening[20] and ∼700 K on the basis of a change in the temperature-dependence of intensity and frequency for a Raman peak.[34] Here, the onset of softening of the shear modulus has been found to occur between 600 and 700 K (Fig. 5), consistent with these previous suggestions for the value of $T_{\rm d}$. Three different mechanisms be considered in more detail-bilinear coupling, softening of optical phonons, and Vogel-Fulcher-like dynamics.

Bilinear coupling between a symmetry-breaking shear strain and the driving order parameter for a (pseudo-proper) ferroelastic transition gives softening of a shear elastic constant, ΔC, as $C\ (T - T_{\rm c})/(T - T_{\rm o})$. Here $T_{\rm c}$ would be the critical temperature as renormalized by coupling with the strain (close to $T_{\rm trans}$) and $T_{\rm o}$ the transition temperature in the absence of bilinear coupling between P and the strain. This does not describe our observed softening of the shear modulus.

Alternatively, based on the Born-Huang long-wavelength approximation and reviewed by Carpenter and Salje,[63] the influence of elastic fluctuations related to a soft mode leads to a power law relationship for softening of elastic constants These elastic fluctuations were predicted by Carpenter and Salje[63] based on the Born-Huang long-wavelength approximation to follow a power law

$$\Delta C \sim (T - T_c)^{\kappa} \tag{1}$$

where T_c is a temperature (below the transition temperature T_{trans}) and κ has values between -1.5 and -0.5 depending on the character of the elastic softening, and, in particular, on the dimension of the phonon mode softening in k-space. As shown in Figure 8a, Eq. 1 provides an adequate description of softening of the shear modulus, expressed as Δf^2, with $T_{\rm c} = 276$ K and $\kappa = -0.5$, which would be consistent with fluctuations occurring in three dimensions. Here, Δf^2 is the squared frequency of the resonance mode relative to its highest value at high temperature. The error due to thermal expansion is also taken into account during the fit of Eq. 1, as described in the caption of Fig. 8.

Another possible softening mechanism relates to thermally activated processes, which as a piece of empiricism might lead to a Vogel-Fulcher relationship

$$\Delta C \sim \exp\left(\frac{E_a}{T - T_{\rm VF}}\right), \tag{2}$$

where E_a is an effective activation energy and $T_{\rm VF}$ is a freezing temperature.[40] As seen in Fig. 8b, this also provides an adequate description of the effective variation of the shear modulus with $T_{\rm VF} = 220.38$ K, $E_a = 72.45$ K. Values of $T_{\rm VF}$ and E_a in the vicinity of 270 K

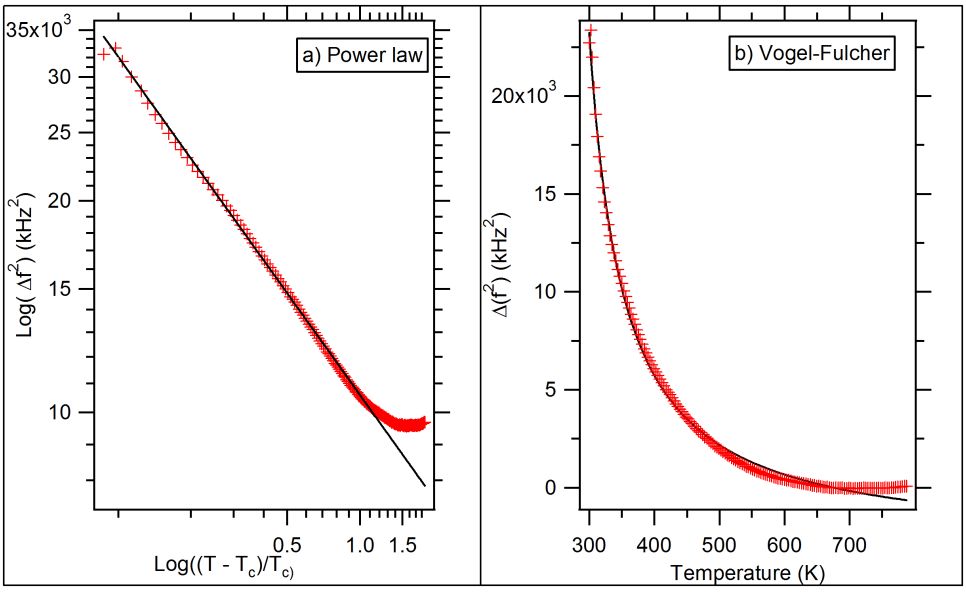

FIG. 8. Temperature evolution of the squared frequency of the resonance frequency and the theoretical fits using a) Power law and b) Vogel-Fulcher relation. For the power law, $A_0 \times (T - T_c)^{\kappa} - B$, the fit parameters are $A_0 = 1.583210^5$ kHz^2, $T_c = 275.85$ K, $\gamma = 0.48$, $B = 9607.6$ kHz^2. For Vogel-Fulcher relation, $A_0 \times \exp\left(\frac{E_a}{T - T_{\rm VF}}\right) - B$, the fit parameters are $A_0 = 17669$ kHz^2, $T_{\rm VF} = 220.38$ K, $E_a = 72.447$ K, and $B = 20719$ kHz^2. For parts **a)** and **b)** Δf^2 corresponds to the difference between the maximum value of the squared resonance frequency, $f^2 = (115780)$ kHz^2, obtained at 600-660 K and those obtained at temperatures between $T_{\rm trans}$ and 800 K. The coefficient B was used to compensate for the error in the baseline due to thermal expansion.

are obtained from more conventional dielectric data from a disordered sample,[27] and it is not possible on this basis of fits to the data shown in Figure 8 to distinguish this from a power law solution.

In PMN elastic softening of the shear modulus in the temperature interval between $T_{\rm d}$ and $T_{\rm m}$ can be represented by Eq. 2 with values of the Vogel-Fulcher parameters that are not unreasonable in comparison with others in the literature from more conventional treatments.[41] Both $C_{11} - C_{12}$ and C_{44}, which make up the shear modulus, each show the same pattern of softening.[41,77,78] Single crystal values of C_{11}, C_{12} and C_{44} for PST given by Fedoseev et al.[56] show that the largest softening at a relatively high degree of disorder ($Q_{\rm od} = 0.29$) would be for the bulk modulus, $1/2(C_{11} + 2C_{12})$, but $1/2(C_{11} - 2C_{12})$ would also have a broad minimum in the vicinity of 280 K. By way of contrast C_{44} has a 50 K interval of softening

below ∼450 K but is then more nearly independent of temperature. It was argued by Carpenter et al.[40] that these symmetry-adapted combinations reflect, separately, local structural variations which have volume strains or tetragonal/orthorhombic and rhombohedral shear strains, respectively. If follows that for PMN the dynamical behavior involved, in effect, is flipping of local dipoles between both tetragonal (and/or orthorhombic) and rhombohedral twin orientations. The anomaly in C_{44} for PST between 400 K and 450 K must reflect local coupling of relaxational modes with the shear strain for rhombohedral distortions, e_4, while the anomaly in $1/2(C_{11} - 2C_{12})$ must reflect coupling of locally tetragonal or orthorhombic relaxational modes. On this basis, the local structural variations near 450 K must at least involve rhombohedral distortions, but perhaps the variations more broadly are associated with flipping between locally tetragonal or orthorhombic domains. There are clear differences between the relatively steep softening and sharp minimum in elastic constants in relatively well ordered samples (this study and Ref. 20) and a much broader, shallower minimum in a relatively disordered sample.[56] This comparison supports the view that there are significant differences between the dynamical behavior of relaxor PST with relatively low degrees of B-site ordering and that of the more normal ferroelectric PST with relatively high degrees of order.

VII. DISCUSSION AND CONCLUSIONS

Our RPS experiments show that PST evolves through a series of distinct regimes in terms of elastic and anelastic behaviour. The low temperature phase is ferroelectric and is strongly RPS active. On heating through the rhombohedral↔cubic transition we have found an interval for phase coexistence of ∼4 K. This is fully explained by the slightly first-order character of the phase transition and has nothing to do with any relaxor properties of the sample. Above $T_{\rm trans}$ the sample is RPS active up to ∼425 K, with precursor elastic softening which extends up to $T_{\rm d}$.

The most interesting result relates to the polar properties of the nominally cubic phase at temperatures below 425 K. In this temperature regime, we find large thermal fluctuations (Fig. 6) and a strong coupling between the local order parameter P and strain. Such couplings give rise to fluctuating micro-structures and it is proposed that these could be manifested as a tweed pattern between 425 K and $T_{\rm trans}$.

The proposed scenario is indirectly supported by other experimental observations than RPS. Refs. 79 and 80 and 29 have shown that transverse polarized diffuse streaking in certain relaxors could be elucidated by Pb displacements that result in polar domains, in addition to off-centering of the B-cations. In samples with low Q_{od}, satellite reflections observed at low temperatures were associated with lead displacements. Further continuous diffuse streaks propagate along directions which coincide with the satellites as is typical for tweed structures.[81] The diffuse streaks were argued to originate from Pb displacements on the (110) planes resulting in polar nanodomains.[34,80,82] Off-centering of the A and B positions was also discussed by Waeselmann et al.[83] who assumed that Pb-based B-site complex perovskite-type relaxor systems might be nanoscale frustrated ferrielectrics. In this case, regions with a spontaneous polarization should contain B-site cation order. This argument agrees with the observation of highly B-site ordered regions in disordered (1 - x)Pb(Sc,Ta)O_{3-x}-(x)$PbTiO_3$ using x-ray absorption spectroscopy.[84]

In summary, we find that PST contains strong polar precursor effects while no classic relaxor behavior was found. For the interpretation of RPS results, we have used a phenomenological Landau model taking into account octahedral distortions, cation off-centering, B-site ordering, heterogeneities in the sample and coupling between these ordering mechanisms. Our analysis indicates that polar tweed formation is possible if the coupling between P and Q is strong.

We can now return to the PNR scenario. In a very vague way, a tweed onset temperature would be similar to the Burns temperature where the first polar clusters nucleate on cooling. The physical picture is somewhat different, however: on cooling through T_{onset} the long range fluctuations increase in amplitude and are already highly coherent. This eliminates the need for a second characteristic temperature T^* where PNR's become coherent. Nevertheless, the two scenarios, tweed and PNR's, are related:[81] when tweed patterns sharpen up and the soft polar regions, such as intersections of the cross weaved strain fields, become patches with more defined boundaries, they would be akin to PNR's. Evidence for such correlations comes from acoustic emission, AE, experiments (Dul'kin et al.[21]) and it would be a test for the existence of tweed (rather than PNR's) in highly ordered material to explore the AE activity as a function of Q_{od}, i.e. the degree of Sc/Ta ordering. Tweed formation would lead to little additional correlation in highly ordered PST while PNR's require strong AE signatures.

Finally, this study demonstrates that RPS is quite sensitive to polar nanostructures, which could make RPS one of the main characterization techniques for the optimization of functional materials such as ferroic and multiferroic materials.

VIII. ACKNOWLEDGEMENTS

Mr. P.C. Osbond is thanked for fabricating the ceramic sample used. RUS facilities in Cambridge were established through support from the NERC (NE/B505738/1) to MAC. EKHS thanks the Leverhulme foundation (RG66640) and EPSRC (RG66344) for financial support.

Appendix: LANDAU THEORY

The Gibbs free energy is the superposition of all energies and the coupling between $Q_{\rm od}$ and Q and P.

$$\begin{aligned} G(Q_{\rm od}, Q, P, e, E) = & L(Q_{\rm od}) + L(Q) + L(P) + G(e) \\ & + G(Q, e) + G(P, Q) + G(Q_{\rm od}, P) \\ & + G(Q_{\rm od}, Q) - PE \end{aligned} \tag{A1}$$

We ignore all other couplings. The individual Landau potentials in the low temperature approximation and scalar representation are[26]

$$\begin{aligned} L(Q_{\rm od}) = & \frac{1}{2} A_{\rm od} \Theta_S^{\rm od} (\frac{\coth \Theta_S^{\rm od}}{T} - \frac{\coth \Theta_S^{\rm od}}{T_c^{\rm od}}) Q_{\rm od}^2 + \frac{1}{4} B_{\rm od} Q_{\rm od}^4 \\ & + \frac{1}{6} C_{\rm od} Q_{\rm od}^6 + \frac{1}{2} g_{\rm od} (\bigtriangledown Q_{\rm od})^2 \end{aligned} \tag{A2}$$

$$\begin{aligned} L(Q) = & \frac{1}{2} A_Q \Theta_S^Q (\frac{\coth \Theta_S^Q}{T} - \frac{\coth \Theta_S^Q}{T_c^Q}) Q^2 + \frac{1}{4} B_Q Q^4 \\ & + \frac{1}{6} C_Q Q^6 + \frac{1}{2} g_Q (\bigtriangledown Q)^2 \end{aligned} \tag{A3}$$

and

$$\begin{aligned} L(P) = & \frac{1}{2} A_P \Theta_S^P (\frac{\coth \Theta_S^P}{T} - \frac{\coth \Theta_S^P}{T_c^P}) P^2 + \frac{1}{4} B_P P^4 \\ & + \frac{1}{6} C_P P^6 + \frac{1}{2} g_P (\bigtriangledown P)^2. \end{aligned} \tag{A4}$$

where indices relate the coefficients and variables to the individual order parameters $Q_{\rm od}$, Q and P. In Eqs. A2-A4 B and C are constants whereas θ_S is the quantum saturation temperature. The coefficient g is used in the Gibbs free energy to include heterogeneities associated with the sample and $g = 0$ when the sample is homogeneous. In addition, $A_{\rm od} = a_{\rm od}(T - T_o)$ for high temperatures, $a_{\rm od}$ is a constant and T_o is the transition temperature in the absence of coupling between the order parameters. The definitions of A_Q and A_P are analogous to $A_{\rm od}$. The quantum saturation temperatures will not be identical for the different order parameters, but their temperature range will be similar for the more displacive parameters Q and P. $Q_{\rm od}$ may have a much higher saturation temperature[26,58,85].

The complete form of the Landau potentials involves the three component of the irreducible representation of $Fm\overline{3}m$. This is

$$\begin{aligned} L(P) = &\frac{1}{2}\alpha(P_1^2 + P_2^2 + P_3^3) + \frac{1}{2}B'(P_1^4 + P_2^4 + P_3^4) \\ &+ B''(P_1^2P_2^2 + P_2^2P_3^2 + P_1^2P_3^2) + \frac{1}{6}C'(P_1P_2P_3)^2 \\ &+ \frac{1}{6}C''(P_1^2 + P_2^2 + P_3^3)^3 + \frac{1}{6}C''(P_1^2 + P_2^2 + P_3^3) \\ &(P_1^4 + P_2^4 + P_3^4) \end{aligned} \tag{A5}$$

and equivalently for the other order parameters. In Eq. A5, $\alpha = a(T - T_o)$ for high temperatures. B', B'', C', C'' and C''' are constants. The components of P are taken in the three [111] directions. The same holds for Q where the components relate to rotations around the individual [111] axes. As we are interested first in the mono-domain state we suppress the component notation and identify the scalar order parameter as the relevant order parameter in one domain.

The coupling between $Q_{\rm od}$ and Q and P is bi-quadratic by symmetry (ignoring the tipping of the P axis):

$$G_{\rm coupling}(Q_{\rm od}, Q) = \lambda_Q Q_{\rm od}^2 Q^2 \tag{A6}$$

$$G_{\rm coupling}(Q_{\rm od}, P) = \lambda_P Q_{\rm od}^2 P^2, \tag{A7}$$

with λ_Q and λ_P being coupling coefficients. In addition, the coupling between Q and P is assumed to be strain induced[24,67,86] with $e \sim Q^2$ and $e \sim P^2$:

$$G_{\rm coupling}(P, e) = \delta_i^P e_i P^2 \tag{A8}$$

$$G_{\rm coupling}(Q, e) = \delta_i^Q e_i Q^2, \tag{A9}$$

where δ_i^P and δ_i^Q are also coupling coefficients.

The elastic energy is given as usual in terms of elastic constants C_{ij} and strains e_i and e_j $(i, j = 1 - 6)$

$$G(e) = \frac{1}{2} C_{ik} e_i e_k. \tag{A10}$$

with summation over repeated indices implied.

The electric response is given by

$$G(P, E) = -\frac{1}{2} \sum \epsilon_{ij} P_j E_k, \tag{A11}$$

with ϵ_{ij}, P_j, and E_k representing the components of the dielectric constant, polarization, and electric field (i, j = 1-3). The piezoelectric effects are derived in lowest order from

$$G(e, P, E) = \sum \xi_{ijkl} e_{ij} \epsilon_{kl} P_l E_k. \tag{A12}$$

where ξ is a constant. The piezoelectric coefficient is then

$$\begin{aligned} d_{ijk} &= -\sum \frac{\partial^2 G}{\partial e_{ij} \partial E_k} = \sum \xi_{ilk} P_l \epsilon_{kj} \\ &\text{or } < d > \approx < \epsilon > < P > \text{ or } < P > \approx \frac{< d >}{< \epsilon >} \end{aligned} \tag{A13}$$

The main effect of B-site ordering is that the transition temperatures T_Q and T_P shift with increasing $Q_{\rm od}$ and that the unit cell enlarges from $Pm\overline{3}m$ to $Fm\overline{3}m$. The octahedral tilt operates on the template of the enlarged cell so that the total distortion has the same translational symmetry as Q and P. In the present study $Q_{\rm od}$ did not change during the experiments and its possible temperature dependence is therefore ignored. It is understood simply that P and Q relax to accommodate to $Q_{\rm od} = 0.65$.

If we focus on the effective bi-quadratic coupling between Q and P, minimizing the total Gibbs free energy with respect to the strain e leads to

$$\begin{aligned} G(Q, P, e = e_{\rm relax}) &= L(Q) + L(P) + \lambda P^2 Q^2 \\ &+ G(e_{\rm relax}) + G_{\rm coupling}(P, e_{\rm relax}) \\ &+ G_{\rm coupling}(Q, e_{\rm relax}) \end{aligned} \tag{A14}$$

---

[1] R. W. Whatmore, Rep. Prog. Phys. **49**, 1335 (1986).

[2] A. Bokov and Z.-G. Ye, J. Mater. Sci. **41**, 31 (2006).

[3] D. J. Lockwood, R. S. Katiyar, and V. C. Y. So, Phys. Rev. B **28**, 1983 (1983).

[4] R. Blinc, A. Gregorovič, B. Zalar, R. Pirc, V. V. Laguta, and M. D. Glinchuk, Phys. Rev. B **63**, 024104 (2000)

[5] V. Westphal, W. Kleemann, and M. D. Glinchuk, Phys. Rev. Lett. **68**, 847 (1992).

[6] D. J. Lockwood, R. S. Katiyar, and V. C. Y. So, Phys. Rev. B **28**, 1983 (1983).

[7] D. La-Orauttapong, J. Toulouse, Z.-G. Ye, W. Chen, R. Erwin, and J. L. Robertson, Phys. Rev. B **67**, 134110 (2003).

[8] O. Svitelskiy, J. Toulouse, G. Yong, and Z.-G. Ye, Phys. Rev. B **68**, 104107 (2003).

[9] B. Dkhil, P. Gemeiner, A. Al-Barakaty, L. Bellaiche, E. Dul'kin, E. Mojaev, and M. Roth, Phys. Rev. B **80**, 064103 (2009).

[10] M. Paściak, T. R. Welberry, J. Kulda, M. Kempa, and J. Hlinka, Phys. Rev. B **85**, 224109 (2012).

[11] J. Hlinka, J. Adv. Dielectr. **02**, 1241006 (2012).

[12] E. K. H. Salje, M. A. Carpenter, G. F. Nataf, G. Picht, K. Webber, J. Weerasinghe, S. Lisenkov, and L. Bellaiche, Phys. Rev. B **87**, 014106 (2013).

[13] B. P. Burton, E. Cockayne, and U. V. Waghmare, Phys. Rev. B **72**, 064113 (2005).

[14] W. W. Schmahl, A. Putnis, E. Salje, P. Freeman, A. Graeme-Barber, R. Jones, K. K. Singh, J. Blunt, P. P. Edwards, J. Loram, et al., Philos. Mag. Lett. **60**, 241 (1989).

[15] B. J. Maier, T. Steilmann, M. Gospodinov, U. Bismayer, and B. Mihailova, J. Appl. Phys. **112**, 124111 (pages 6) (2012).

[16] C. G. F. Stenger, F. L. Scholten, and A. J. Burggraaf, Solid State Commun. **32**, 989 (1979).

[17] C. G. F. Stenger and A. J. Burggraaf, Phys. Status Solidi A **61**, 275 (1980).

[18] C. G. F. Stenger and A. J. Burggraaf, Phys. Status Solidi A **61**, 653 (1980).

[19] N. Setter and L. E. Cross, J. Appl. Phys. **51**, 4356 (1980).

[20] V. Sivasubramanian and S. Kojima, Phys. Rev. B **85**, 054104 (2012).

[21] E. Dul'kin, B. Mihailova, G. Catalan, M. Gospodinov, and M. Roth, Phys. Rev. B **82**, 180101 (2010).

[22] E. Dul'kin, B. Mihailova, M. Gospodinov, and M. Roth, EPL **94**, 57002 (2011).

[23] K. Z. Baba-Kishi and M. Pasciak, J. Appl. Cryst. **43**, 140 (2010).

[24] A. M. Bratkovsky, S. C. Marais, V. Heine, and E. K. H. Salje, J. Phys.: Condens. Matter **6**,

3679 (1994).

[25] K. Parlinski, V. Heine, and E. K. H. Salje, J. Phys.: Condens. Matter **5**, 497 (1993).

[26] E. Salje, B. Wruck, and H. Thomas, Z. Phys. B **82**, 399 (1991).

[27] F. Chu, N. Setter, and A. K. Tagantsev, J. Appl. Phys. **74**, 5129 (1993).

[28] P. Groves, J. Phys. C: Solid State Phys. **18**, L1073 (1985).

[29] P. M. Woodward and K. Z. Baba-Kishi, J. Appl. Crystallogr. **35**, 233 (2002).

[30] B. J. Maier, R. J. Angel, W. G. Marshall, B. Mihailova, C. Paulmann, J. M. Engel, M. Gospodinov, A.-M. Welsch, D. Petrova, and U. Bismayer, Acta Cryst. B **66**, 280 (2010).

[31] J. Peng and L. A. Bursill, Mod. Phys. Lett. B **7**.

[32] L. Kamzina and N. Krainik, Phys. Sol. State **42**, 142 (2000).

[33] F. Chu, I. M. Reaney, and N. Setter, J. Am. Ceram. Soc. **78**, 1947 (1995).

[34] B. Mihailova, B. Maier, C. Paulmann, T. Malcherek, J. Ihringer, M. Gospodinov, R. Stosch, B. Güttler, and U. Bismayer, Phys. Rev. B **77**, 174106 (2008).

[35] L. Landau and E. Lifshitz, *Statistical Physics*, v. 5 (Elsevier Science, 1996), ISBN 9780080570464.

[36] A. Migliori and J. Sarrao, *Resonant ultrasound spectroscopy: applications to physics, materials measurements, and nondestructive evaluation* (Wiley, 1997).

[37] R. E. A. McKnight, T. Moxon, A. Buckley, P. A. Taylor, T. W. Darling, and M. A. Carpenter, J. Phys.: Condens. Matter **20**, 075229 (2008).

[38] M. A. Carpenter, A. Buckley, P. A. Taylor, R. E. A. McKnight, and T. W. Darling, J. Phys.: Condens. Matter **22**, 035406 (2010).

[39] E. K. H. Salje and M. A. Carpenter, Appl. Phys. Lett. **99**, 051907 (pages 3) (2011).

[40] M. A. Carpenter, J. F. J. Bryson, G. Catalan, and C. J. Howard, J. Phys.: Condens. Matter **24**, 045901 (2012).

[41] M. A. Carpenter, J. F. J. Bryson, G. Catalan, S. J. Zhang, and N. J. Donnelly, J. Phys.: Condens. Matter **24**, 045902 (2012).

[42] P. C. Osbond and R. W. Whatmore, Ferroelectrics **133**, 159 (1992).

[43] N. M. Shorrocks, R. W. Whatmore, and P. C. Osbond, Ferroelectrics **106**, 387 (1990).

[44] R. W. Whatmore, N. Shorrocks, P. C. Osbond, S. Stringfellow, C. F. Carter, and R. Watton, in *ISAF '92., Proc. Eighth IEEE Inter. Symp. Appl. Ferroelec.* (Aug-2 Sep), pp. 202–205.

[45] A. Cohelo, *TOPAS-Academic* (Coelho Software, 2007).

[46] R. E. McKnight, M. A. Carpenter, T. W. Darling, A. Buckley, and P. A. Taylor, Am. Mineral. **92**, 1665 (2007).

[47] B. J. Maier, N. Waeselmann, B. Mihailova, R. J. Angel, C. Ederer, C. Paulmann, M. Gospodinov, A. Friedrich, and U. Bismayer, Phys. Rev. B **84**, 174104 (2011).

[48] B. Mihailova, R. Angel, B. Maier, A. Welsch, J. Zhao, M. Gospodinov, and U. Bismayer, IEEE Trans. Ultrason Ferroelectr. Freq. Control **58**, 1905 (2011).

[49] Z. Zhao, X. Ding, T. Lookman, J. Sun, and E. K. H. Salje, Adv. Mater. **25**, 3244 (2013).

[50] E. K. H. Salje, H. Zhang, H. Idrissi, D. Schryvers, M. A. Carpenter, X. Moya, and A. Planes, Phys. Rev. B **80**, 134114 (2009).

[51] J. F. Scott, E. K. H. Salje, and M. A. Carpenter, Phys. Rev. Lett. **109**, 187601 (2012).

[52] M. A. Carpenter and E. K. H. Salje, Eur. J. Mineral. **10**, 693 (1998).

[53] W. J. Merz, Phys. Rev. **91**, 513 (1953).

[54] S. Bains, P. C. Osbond, R. W. Whatmore, and F. Ainger, in *Proc. of British Cer. Soc. No: 36* (1985), pp. 67–78.

[55] K. Z. Baba-Kishi and D. J. Barber, J. Appl. Crystallogr. **23**, 43 (1990).

[56] A. Fedoseev, S. Lushnikov, S. Gvasaliya, and S. Kojima, Phys. Solid State **48**, 1102 (2006).

[57] E. Salje and U. Bismayer, J. Phys.: Condens. Matter **1**, 6967 (1989).

[58] S. A. Hayward and E. K. H. Salje, J. Phys.: Condens. Matter **10**, 1421 (1998).

[59] E. K. H. Salje, M. C. Gallardo, J. Jimnez, F. J. Romero, and J. del Cerro, J. Phys.: Condens. Matter **10**, 5535 (1998).

[60] B. J. Maier, R. J. Angel, B. Mihailova, W. G. Marshall, M. Gospodinov, and U. Bismayer, J. Phys.: Condens. Matter **23**, 035902 (2011).

[61] B. Mihailova, N. Waeselmann, B. J. Maier, R. J. Angel, T. Prmann, C. Paulmann, M. Gospodinov, and U. Bismayer, J. Phys.: Condens. Matter **25**, 115403 (2013).

[62] B. Mihailova, R. J. Angel, A.-M. Welsch, J. Zhao, J. Engel, C. Paulmann, M. Gospodinov, H. Ahsbahs, R. Stosch, B. Güttler, et al., Phys. Rev. Lett. **101**, 017602 (2008).

[63] M. A. Carpenter, E. K. H. Salje, and A. Graeme-Barber, Eur. J. Mineral. **10**, 621 (1998).

[64] E. Salje and V. Devarajan, J. Phys. C: Sol. State Phys. **14**, L1029 (1981).

[65] E. K. H. Salje, A. Graeme-Barber, M. A. Carpenter, and U. Bismayer, Acta Cryst. B **49**, 387 (1993).

[66] E. K. Salje, D. J. Safarik, J. C. Lashley, L. A. Groat, and U. Bismayer, Am. Mineral. **96**, 1254

(2011).

[67] B. Houchmandzadeh, J. Lajzerowicz, and E. Salje, J. Phys.: Condens. Matter **3**, 5163 (1991).

[68] S. Conti, S. Mller, A. Poliakovsky, and E. K. H. Salje, J. Phys.: Condens. Matter **23**, 142203 (2011).

[69] E. K. H. Salje, ChemPhysChem **11**, 940 (2010).

[70] M. Calleja, M. T. Dove, and E. K. H. Salje, J. Phys.: Condens. Matter **15**, 2301 (2003).

[71] L. Goncalves-Ferreira, S. A. T. Redfern, E. Artacho, and E. K. H. Salje, Phys. Rev. Lett. **101**, 097602 (2008).

[72] A. N. Morozovska, E. A. Eliseev, M. D. Glinchuk, L.-Q. Chen, and V. Gopalan, Phys. Rev. B **85**, 094107 (2012).

[73] S. Van Aert, S. Turner, R. Delville, D. Schryvers, G. Van Tendeloo, and E. K. H. Salje, Adv. Mater. **24**, 523 (2012).

[74] G. W. Milton, *The Theory of Composites*, vol. 6 of *Cambridge monographs on applied and computational mathematics* (2002), ISBN 0-521-78125-6.

[75] E. Salje and K. Parlinski, Superconductor Science and Technology **4**, 93 (1991).

[76] X. Meng, K. Z. Baba-Kishi, G. K. H. Pang, H. L. Chan, C. L. Choy, and H. S. Luo, Philos. Mag. Lett. **84**, 191 (2004).

[77] N. K. Y. G. A. Smolenskii and S. N. Smirnov, Sov. Phys/Solid State **27**, 492 (1985).

[78] S. G. Lushnikov, A. I. Fedoseev, S. N. Gvasaliya, and S. Kojima, Phys. Rev. B **77**, 104122 (2008).

[79] K. S. Knight and K. Z. Baba-kishi, Ferroelectrics **173**, 341 (1995).

[80] C. Randall, D. Barber, R. Whatmore, and P. Groves, J. Mat. Sci. **21**, 4456 (1986).

[81] E. K. H. Salje, X. Ding, Z. Zhao, and T. Lookman, Appl. Phys. Lett. **100**, 222905 (pages 3) (2012).

[82] T. R. Welberry and D. J. Goossens, Acta Cryst. A **64**, 23 (2008).

[83] N. Waeselmann, B. Mihailova, B. J. Maier, C. Paulmann, M. Gospodinov, V. Marinova, and U. Bismayer, Phys. Rev. B **83**, 214104 (2011).

[84] A. I. Frenkel, D. M. Pease, J. Giniewicz, E. A. Stern, D. L. Brewe, M. Daniel, and J. Budnick, Phys. Rev. B **70**, 014106 (2004).

[85] S. A. Hayward and E. K. H. Salje, J. Phys.: Condens. Matter **14**, L599 (2002).

[86] S. Marais, V. Heine, C. Nex, and E. Salje, Phys. Rev. Lett. **66**, 2480 (1991).